

# Duality Between Relaxation and First Passage in Reversible Markov Dynamics: Rugged Energy Landscapes Disentangled

**David Hartich and Aljaž Godec**

Mathematical Biophysics Group, Max-Planck-Institute for Biophysical Chemistry,  
Göttingen 37077, Germany

E-mail: [david.hartich@mpibpc.mpg.de](mailto:david.hartich@mpibpc.mpg.de), [agodec@mpibpc.mpg.de](mailto:agodec@mpibpc.mpg.de)

**Abstract.** Relaxation and first passage processes are the pillars of kinetics in condensed matter, polymeric and single-molecule systems. Yet, an explicit connection between relaxation and first passage time-scales so far remained elusive. Here we prove a duality between them in the form of an interlacing of spectra. In the basic form the duality holds for reversible Markov processes to effectively one-dimensional targets. The exploration of a triple-well potential is analyzed to demonstrate how the duality allows for an intuitive understanding of first passage trajectories in terms of relaxational eigenmodes. More generally, we provide a comprehensive explanation of the full statistics of reactive trajectories in rugged potentials, incl. the so-called ‘few-encounter limit’. Our results are required for explaining quantitatively the occurrence of diseases triggered by protein misfolding.

## 1. Introduction

Relaxation dynamics are a paradigm for describing complex dynamical phenomena spanning condensed matter [1], polymeric [2], granular [3] and single-molecule systems [4, 5], and even cellular regulatory networks [6]. Relaxation concepts underlie most spectroscopic methods [1]. Moreover, our understanding of metastability is built entirely on the properties of relaxation spectra [7–11]. Complementary to relaxation processes are the statistics of the first passage time, the time a random process reaches a prescribed threshold value for the first time. First passage time statistics in turn are central to the kinetics of chemical reactions [12–22], signaling in biological cells [20–31], transport in disordered media [32], the foraging behavior of bacteria and animals [33–35], up to the spreading of diseases [36, 37] or stock market dynamics [38]. Further important applications of first passage concepts include the persistence properties in non-equilibrium systems [39–41] and stochastic thermodynamics [42–47].

Both relaxation and first passage processes are essential for theories building on a diffusive exploration of (free) energy landscapes  $U(x)$  [48], which have proven to be particularly invaluable in explaining the kinetics of chemical reactions [49, 50], protein dynamics [51, 52] incl. recent single protein folding experiments [53], and the dynamics

of supercooled liquids and glasses [9–11, 54]. Whereas relaxation processes can be understood intuitively in terms of the eigenmodes and eigenvalues of the underlying Fokker-Planck or Kramers operators [9–11, 55], general, and in particular intuitive results about the full first passage time statistics are much sparser, and currently do not reach beyond a crude division between so-called direct and indirect first-passage trajectories for the simplest smooth potential landscapes [17, 20, 24, 26, 27]. Our general understanding of first passage phenomena would therefore substantially benefit from a deeper connection to the corresponding relaxation process.

Indeed, in the limit of high energy barriers a well-known link relates  $\lambda_1^{-1}$ , the longest relaxation time, and the mean first passage time to surmount the highest barrier in the landscape [7–11, 56]. However, in spite of the immense success and universal applicability of this approximate relationship, an explicit bridge between first passage and relaxation time-scales has not been explored further.

Here we establish such a link rigorously for microscopically reversible Markovian dynamics. We prove that the first-passage process to an effectively one-dimensional target is in fact the *dual* to the corresponding relaxation process. The duality takes the form of a *spectral interlacing* of characteristic time-scales, in which each pair of successive relaxation time-scales encloses a first-passage time-scale. We establish an explicit relationship between relaxation and first-passage spectra, and express the full statistics of first passage time exactly in terms of the relaxation eigensystem. As a case study we consider a diffusive exploration of a triple-well potential. Moreover, exploiting the duality we disentangle first passage time statistics in general rugged energy landscapes. We argue why our results are important for a quantitative understanding of the occurrence of diseases related to protein misfolding.

The paper is organized as follows. In Sec. 2 we expose the duality between first passage and relaxation processes. In Sec. 3 we determine the first passage time statistics in a simple triple-well potential and demonstrate that knowing the full probability density is mandatory in studies of many-particle first passage problems in the few encounter limit. In Sec. 4 we determine the first passage time density for a truly rugged energy landscape generated by a truncated Karhunen-Loève expansion of a Wiener process. The large deviation limit of the first passage time distribution, which is relevant for single-molecule first passage problems, is presented in Sec. 5. We conclude in Sec. 6. A proof of the duality between first passage and relaxation is relegated to Appendix A.

## 2. First passage time density from the relaxation spectrum

We consider reversible Markovian dynamics in continuous time governed by a Fokker-Planck operator  $\mathbf{L} = \partial_x D(x) [\beta U'(x) + \partial_x]$ , where  $x$  is the position,  $U(x)$  a potential with  $U'(x) \equiv \partial_x U(x)$ , and  $D(x)$  the diffusion landscape. We assume  $\beta$  to be the inverse temperature, such that according to the fluctuation-dissipation theorem  $\beta D(x)$  is the inverse friction coefficient. For any initial condition  $x_0$  the dynamics governed by the Fokker-Planck operator  $\mathbf{L}$  relaxes to the Boltzmann distribution  $P_{\text{eq}}(x) =$

$e^{-\beta U(x)} / \int e^{-\beta U(x)} dx$ . Adopting the bra-ket notation we expand  $\mathbf{L}$  in a complete bi-orthogonal set of left and right eigenstates,  $\mathbf{L} = -\sum_k \lambda_k |\psi_k^R\rangle \langle \psi_k^L|$ ,  $\lambda_k$  denoting the eigenvalues and  $\langle \psi_k^L | \psi_l^R \rangle = \delta_{kl}$  with  $|\psi_k^L\rangle \equiv e^{\beta U(x)} |\psi_k^R\rangle$ . The propagator encoding the probability to be at  $x$  at a time  $t$  after starting from  $x_0$  at  $t_0 = 0$ , is defined as

$$P(x, t|x_0) \equiv \langle x | e^{\mathbf{L}t} | x_0 \rangle = \sum_k \langle x | \psi_k^R \rangle \langle \psi_k^L | x_0 \rangle e^{-\lambda_k t}. \quad (1)$$

Since we assumed temporally homogeneous dynamics, we can define the first passage time probability density from some  $x_0$  to a target at  $a$ ,  $\wp_a(t|x_0)$ , by the renewal theorem [57]

$$P(x, t|x_0) = \int_0^t \wp_a(\tau|x_0) P(x, t-\tau|a) d\tau, \quad (2)$$

where either  $x_0 < a \leq x$ , or symmetrically  $x_0 > a \geq x$ . Eq. (2) follows from a direct enumeration of paths between  $x_0$  and  $x$ , which by construction must pass through  $a$ . Laplace transforming Eq. (2) we obtain  $\tilde{\wp}_a(s|x_0) = \tilde{P}(x, s|x_0) / \tilde{P}(x, s|a)$ , which is the starting point of our analysis. Using Eq. (1), which after Laplace transform reads  $\tilde{P}(x, s|x_0) = \sum_k (s + \lambda_k)^{-1} \langle x | \psi_k^R \rangle \langle \psi_k^L | x_0 \rangle$ , yields

$$\tilde{\wp}_a(s|x_0) = \frac{\sum_k (s + \lambda_k)^{-1} \langle x | \psi_k^R \rangle \langle \psi_k^L | x_0 \rangle}{\sum_k (s + \lambda_k)^{-1} \langle x | \psi_k^R \rangle \langle \psi_k^L | a \rangle}. \quad (3)$$

The Laplace transform of the first passage time density  $\tilde{\wp}_a(s|x_0)$  is a meromorphic function having simple poles  $-\mu_k$  on the negative real axis [58]. Moreover, the poles have no accumulation point in the left half plane ( $\text{Re}(s) < 0$ ). Similarly,  $\tilde{P}(y, s|x)$  is meromorphic with simple poles  $-\lambda_k$  arranged along the non-positive real axis. In particular,  $\lambda_0 = 0$  and  $\langle x | \psi_0^R \rangle \langle \psi_0^L | x_0 \rangle = P_{\text{eq}}(x)$ .

The Laplace transforms of the propagators  $\tilde{P}(x, s|x_0)$  and  $\tilde{P}(x, s|a)$  have coinciding poles, while the poles of  $\tilde{\wp}_a(s|x_0)$  are those zeroes of  $\tilde{P}(x, s|a)$ , which are different from the zeroes of  $\tilde{P}(x, s|x_0)$ . Generally,  $\tilde{P}(x, s|x_0)$  and  $\tilde{P}(x, s|a)$  have infinitely many coinciding zeroes alongside the distinct ones (see proof in [59]), because the region beyond  $a$  cannot affect the first passage time from  $x_0$ , whereas it must affect the relaxation. However, all common zeroes result in a vanishing residue.

One can prove that setting  $x = a$  in Eqs. (2) and (3) guarantees that *all relevant* eigenvalues (i.e., those satisfying  $\langle a | \psi_k^R \rangle \neq 0$ ) of the relaxation and first passage processes interlace

$$\lambda_{k-1} < \mu_k < \lambda_k, \quad \forall k \geq 1, \quad (4)$$

which is due to the fact that  $\langle a | \psi_k^R \rangle \langle \psi_k^L | a \rangle > 0$  (see also [59]). Based on the interlacing in Eq. (4) we are now in the position to determine the entire first passage time statistics from the relaxation eigenspectrum,  $\{|\psi_k^R\rangle, \langle \psi_k^L|, \lambda_k\}$ . The calculation becomes rather involved and is sketched in Appendix A (see also [59]), here we simply state the result. Introducing  $\bar{\mu}_k = (\lambda_k + \lambda_{k-1})/2$  the corresponding first passage eigenvalues  $\mu_k$  are given exactly in the form of a convergent Newton's series

$$\mu_k = \bar{\mu}_k + \sum_{n=1}^{\infty} f_0(k)^n f_1(k)^{1-2n} \frac{\det \mathcal{A}_n(k)}{(n-1)!}, \quad (5)$$

with the almost triangular  $(n-1) \times (n-1)$  matrix  $\mathcal{A}_n(k)$  with elements

$$\mathcal{A}_n^{i,j}(k) = \frac{f_{(i-j+2)}(k)\Theta(i-j+1)}{(i-j+2)!} \left[ n(i-j+1)\Theta(j-2) + i\Theta(1-j) + j-1 \right], \quad (6)$$

where  $\Theta(l)$  denotes the discrete Heaviside step function ( $\Theta(l) = 1$  if  $l \geq 0$ ), and symbolically we set  $\det \mathcal{A}_1 \equiv 1$ . Setting  $k^* = k$  if  $\tilde{P}(a, -\bar{\mu}_k|a) < 0$  and  $k^* = k-1$  otherwise,  $f_n(k)$  in Eqs. (5-6) are defined by

$$\begin{aligned} f_0(k) &= \langle a|\psi_{k^*}^R \rangle \langle \psi_{k^*}^L|a \rangle + \sum_{l \neq k^*} \langle a|\psi_l^R \rangle \langle \psi_l^L|a \rangle \frac{(\bar{\mu}_k - \lambda_{k^*})}{(\bar{\mu}_k - \lambda_l)}, \\ f_{n \geq 1}(k) &= n! \sum_{l \neq k^*} \langle a|\psi_l^R \rangle \langle \psi_l^L|a \rangle \frac{(\lambda_l - \lambda_{k^*})}{(\bar{\mu}_k - \lambda_l)^{n+1}}. \end{aligned} \quad (7)$$

Using Eq. (7) the determinant  $\det \mathcal{A}_n(k)$  of the almost triangular matrix with elements (6) is fully characterized, which in turn determines the first passage eigenvalue Eq. (5). It is now easy to obtain  $\wp_a(t|x_0)$  by inverting the Laplace transform in Eq. (3) using Cauchy's residue theorem yielding [59]

$$\wp_a(t|x_0) = \sum_{k \geq 1} w_k(x_0) \mu_k e^{-\mu_k t}, \quad (8)$$

where the spectral weights as a function of the initial condition  $x_0$ ,  $w_k(x_0)$ , are given by

$$w_k(x_0) = \frac{\sum_l (1 - \lambda_l/\mu_k)^{-1} \langle a|\psi_l^R \rangle \langle \psi_l^L|x_0 \rangle}{\sum_l (1 - \lambda_l/\mu_k)^{-2} \langle a|\psi_l^R \rangle \langle \psi_l^L|a \rangle}, \quad (9)$$

where we only sum over relevant  $\lambda_l$ , and the weights are normalized  $\sum_{k \geq 1} w_k(x_0) = 1$ . Moments of the first passage time follow immediately,

$$\langle t_a^n(x_0) \rangle = n! \sum_{k \geq 1} w_k(x_0) \mu_k^{-n} \quad (10)$$

We note that while the first weight is necessarily positive,  $w_1(x_0) > 0$ , the other weights  $w_k(x_0)$  can be negative for  $k > 1$ . In the following section we will show how this duality between first passage and relaxation can be used to determine and understand more deeply the full first passage time distribution.

For the sake of completeness we briefly comment on the “reverse” direction of the duality. The starting point is the renewal theorem (2) for  $x = a$  in Laplace space, which reads  $\tilde{\wp}_x(s|x_0) = \tilde{P}(x, s|x_0)/\tilde{P}(x, s|x)$ . Using standard Green's function theory [59] it can be shown after some straightforward but tedious algebra that

$$\tilde{P}(x, s|x_0) = \sigma_{\pm} \frac{e^{\beta U(x_0) - \beta U(x)} \tilde{\wp}_{x_0}(s|x)}{D \frac{\partial}{\partial x_0} \ln[\tilde{\wp}_{x_0}(s|x) \tilde{\wp}_x(s|x_0)]} \quad (11)$$

holds, where  $\sigma_{\pm} = -1$  if  $x_0 < x$  and  $\sigma_{\pm} = +1$  if  $x_0 > x$ . For the remainder of the paper we will focus solely on the explicit forward duality, since it allows us to efficiently determine the full first passage time density.

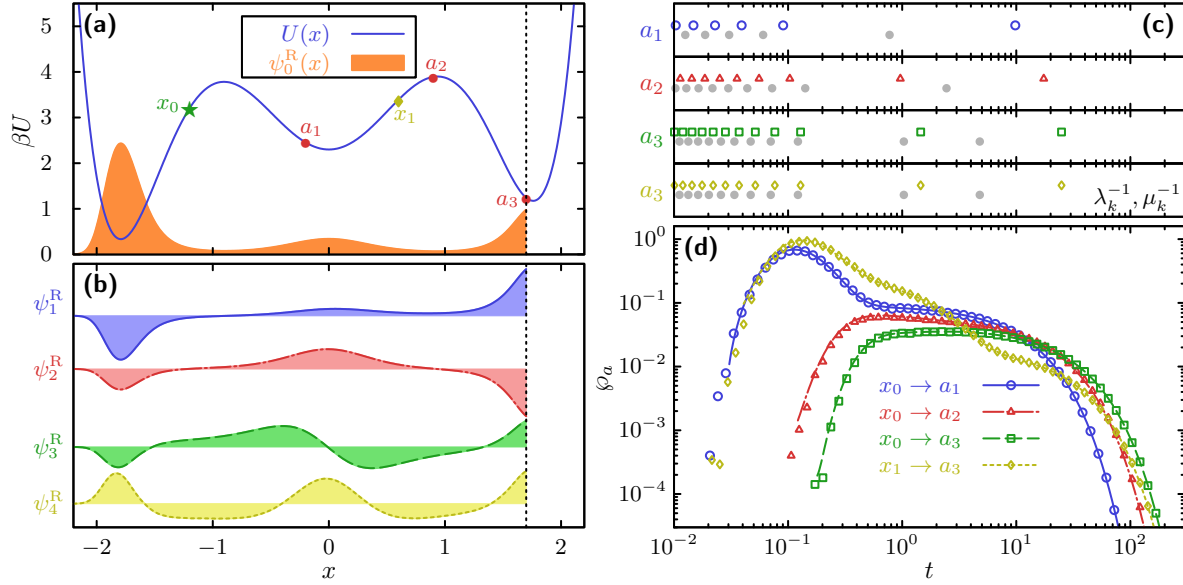


**Figure 1.** (a) Triple well potential  $\beta U(x) = (x^6 - 6x^4 + 0.15x^3 + 8x^2)/2$  (line) and corresponding invariant measure  $P_{\text{eq}}(x) \propto \psi_0^R(x)$  (shaded). Highlighted are the initial conditions  $x_0 = -1.2$  and  $x_1 = 0.6$  alongside three target positions  $a_1 = -0.2$ ,  $a_2 = 0.9$  and  $a_3 = 1.7$ ; (b) Right eigenvectors  $\psi_k^R(x) \equiv \langle x | \psi_k^R \rangle$  for the four slowest eigenmodes of the relaxation process with a reflecting boundary at  $a_3$ ; (c) Spectra of characteristic time scales for relaxation ( $\lambda_k^{-1}$ , filled gray circles), and first passage ( $\mu_k^{-1}$ , open color symbols) processes, with the boundaries at  $a_1$  to  $a_3$ , respectively; we used reflecting boundaries for the determination of  $\lambda_k^{-1}$  and absorbing boundaries for  $\mu_k^{-1}$ ; (d) First passage time probability densities – the lines correspond to Eq. (8) and the symbols to Brownian dynamics simulations each of an ensemble of  $2 \times 10^6$  trajectories with an integration step  $\Delta t = 10^{-5}$ .

### 3. Triple-well potential

#### 3.1. First passage time density

As a case study we analyze the first passage time statistics in a triple well potential (see Fig. 1a). Understanding the diffusive exploration of multi-well potentials is important from a biophysical perspective, as it underlies e.g. the folding [53,60], misfolding [61,62], conformational dynamics [4,5] and aggregation of proteins and peptides [63,64] as well as (bio)chemical reactions [49,50].

We computed the first 40 left and right relaxation eigenvectors,  $\langle x | \psi_k^R \rangle$  and  $\langle \psi_k^L | a \rangle$ , and eigenvalues  $\lambda_k$  numerically using a reflecting boundary condition at the target  $a$ . The four lowest  $\langle x | \psi_k^R \rangle$  of the relaxation process are depicted in Fig. 1b. From  $\{\lambda_k, |\psi_k^R\rangle, \langle \psi_k^L|\}$  we calculate the first 30  $\mu_k$  and  $w_k(x_0)$  using the duality, i.e. Eqs. (5) and (9). The spectrum of first passage eigenvalues is depicted in Fig. 1c, with the corresponding first passage time probability densities shown in Fig. 1d (lines) and compared to the result of Brownian dynamics simulations (symbols). We find an excellent agreement between theory and simulations. Note that the deviations of the theoretical results from simulations observed on extremely short timescales are a direct

consequence of truncating the sums in Eqs. (1) and (8) (i.e., we considered 40 eigenvalues in the relaxation spectrum and 30 first passage eigenvalues).

We now link metastability to the first passage time behavior. A potential  $U(x)$  has metastable states if the minima are separated by high barriers  $> k_B T$ . The probability mass in the ground state  $P_{\text{eq}}(x)$  is concentrated around these minima. The barriers give rise to a separation of time-scales between inter-well (see, e.g.,  $\psi_1^R, \psi_2^R$  in Fig. 1b) and intra-well dynamics (see  $\psi_{k>2}^R$ ), and thus create gaps in the relaxation spectrum [8–11]. As a result we observe in Fig. 1c (see filled gray circles) two gaps  $0 = \lambda_0 \ll \lambda_1 \ll \lambda_2 < \lambda_3$  when the reflecting boundary is at  $a_1$ , corresponding to the crossing of a single barrier. Conversely, three gaps,  $0 \ll \lambda_1 \ll \lambda_2 \ll \lambda_3 < \lambda_4$ , appear when the reflecting boundary is at  $a_3$ , corresponding to the global relaxation to  $P_{\text{eq}}(x)$ , to direct transitions between the leftmost and right-most wells, and to the transition to the central well from both sides, respectively (see Fig. 1b). These gaps are independent of  $x_0$ .

Due to the interlacing (Eq. (4)), and because  $\mu_1 \neq 0$ , the  $N$  gaps in the relaxation spectrum reflecting all the metastable basins translate to  $N - 1$  gaps in the first passage spectrum due to the  $N - 1$  barriers. The first passage spectrum is shifted to shorter times, since contrary to relaxation, *all trajectories* must surmount the barriers. The spectral weights  $w_k$  depend on the initial position, gauging the contribution of each relaxation mode with respect to the given first passage time-scale  $\mu_k^{-1}$  (see Eq. (9)). The four lowest  $w_k$  for the first passage process  $x_0 \rightarrow a_3$  are shown in Fig. 2a.

In view of [26, 27] (see also [20]) we now separate all first passage trajectories into two classes — the so-called ‘globally indirect’ and the rest. The class of ‘globally indirect’ trajectories includes those exploring the entire accessible phase space prior to absorption. These trajectories therefore arrive on the slowest time-scale  $\mu_1^{-1}$  and their associated weight  $w_1$  is approximately the fraction of all first passage trajectories that reach quasi-equilibrium before hitting the target. Correspondingly,  $w_1$  — the weight of globally indirect trajectories decreases as the starting position  $x_0$  approaches the target at  $a$  (see e.g. blue solid line in Fig. 2a for  $a = 1.7$ ). In other words, the closer  $x_0$  is to the target the more unlikely are globally indirect trajectories.

Pushing this picture even further we can also identify in Fig. 1d ( $x_1 \rightarrow a_3$ ) a second pronounced time-scale  $\mu_2^{-1}$  with weight  $w_2$ , reflecting what we may call ‘locally indirect’ trajectories — those that first equilibrate locally within the central well but cross the second barrier without returning to the left, deepest well. Comparing the second weight  $w_2$  from Fig. 2a (see dash-dotted red line) and the potential landscape Fig. 1a we find that ‘locally indirect’ trajectories are most pronounced in the sense of the largest value of  $w_2$  if the starting position is within the central well. The locally indirect trajectories account for local equilibration prior to absorption and become relevant as soon as the potential landscapes has more than one deep free energy basin, such as for example the one depicted in Fig. 1. Our work therefore extends the present understanding of first passage processes [20, 26, 27] by explicitly identifying locally indirect trajectories — those equilibrating only locally prior to absorption.

For  $x_0$  within the central well the fraction of globally indirect trajectories decreases,



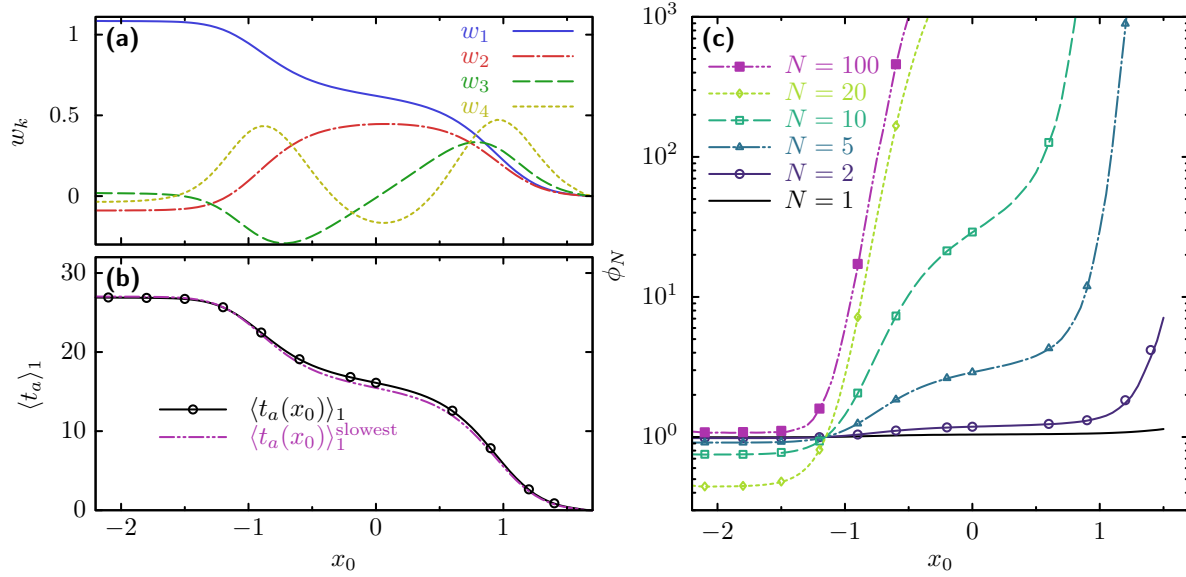


**Figure 2.** First passage in triple-well potential from Fig. 1 to fixed target position  $a_3 = 1.3$ . (a) Lowest four weights  $w_k(x_0)$  determined from Eq. (9) for the first passage process from  $x_0$  to fixed target  $a = a_3$  in the triple-well potential depicted in Fig. 1a as a function of the starting point  $x_0$ . (b) Mean first passage time (solid black line) corroborated by Brownian simulations (symbols) versus slowest time-scale approximation  $\langle t_a(x_0) \rangle_1^{\text{slowest}} = w_1(x_0)/\mu_1$  from Eq. (15). (c)  $\phi_N = \langle t_a(x_0) \rangle_N / \langle t_a(x_0) \rangle_1^{\text{slowest}}$  comparing the mean first passage time of  $N$  particles,  $\langle t_a(x_0) \rangle_N$ , with the one-scale approximation  $\langle t_a(x_0) \rangle_N^{\text{slowest}} = w_1(x_0)^N / (N\mu_1)$  (see Eq. (15)) for various  $N$ . Lines denote the theory and symbols the simulation results.

and locally indirect trajectories become likelier, i.e.  $w_2$  increases. Concurrently, higher spectral weights also grow, rendering direct trajectories more likely. As a result, an additional time-scale appears, giving rise to a second ‘bump’ in  $\wp_a(t)$  (see Fig. 1d, blue lines). This reasoning extends to arbitrary landscapes;  $w_k, \mu_k$  reflect a hierarchy of time-scales, on which trajectories equilibrate locally in the sequence of all intervals between consecutive basins and  $a$ , before hitting  $a$ . The highest modes encode direct trajectories.

### 3.2. Few encounter kinetics require the full first passage time distribution

The full first passage time statistics are crucial for kinetics in the few-encounter limit, when only the first of many particles needs to find the target [26, 27]. We highlight this on hand of first passage time statistics in a non-interacting  $N$ -particle system. The  $N$ -particle survival probability — the probability that none of the  $N$  particles starting from  $x_0$  has reached the target until time  $t$  — is simply given by

$$\mathcal{P}_a(t|x_0)^N \equiv \left[ \int_t^\infty \wp_a(\tau|x_0) d\tau \right]^N = \left[ \sum_{k>0} w_k(x_0) e^{-\mu_k t} \right]^N, \quad (12)$$

where we have inserted Eq. (8). We note that if the initial conditions were not identical with  $x_i \neq x_0$  for all  $i = 1, \dots, N$  one would replace the survival probability  $\mathcal{P}_a(t|x_0)^N$  by

the product  $\prod_{i=1}^N \mathcal{P}_a(t|x_i)$ . For convenience, we will restrict our discussion to the scenario in which all particles start from the same position. Using the survival probability (12) the  $N$ -particle first passage time density follows directly from the single particle case

$$\wp_a^{(N)}(t|x_0) \equiv -\frac{\partial}{\partial t} \mathcal{P}_a(t|x_0)^N = N \wp_a(t|x_0) \mathcal{P}_a(t|x_0)^{N-1}, \quad (13)$$

which is the probability density that one of  $N$  particles reaches the target  $a$  at time  $t$  under the condition that none of the remaining  $N - 1$  particles has arrived before. Obviously,  $N$ -particles will find the target on average in a shorter time than a single particle. More precisely, the mean first passage time in the many particle setting reads

$$\langle t_a(x_0) \rangle_N \equiv \int_0^\infty t \wp_a^{(N)}(t|x_0) dt = \int_0^\infty \mathcal{P}_a(t|x_0)^N dt, \quad (14)$$

where we have inserted Eq. (13) and performed an integration by parts in the last step.

Let us now focus on the mean first passage time and start with a single particle exploration ( $N = 1$ ) in which case the mean according to Eq. (10) is simply given by  $\langle t_a(x_0) \rangle_1 = \sum_{k>0} w_k(x_0)/\mu_k$ . If there are free energy barriers between the initial position of the particle and the target, which lead the emergence of a local equilibrium before reaching  $a$ , i.e.,  $\mu_2 \gg \mu_1$ , we expect the mean first passage time to be well approximated by the slowest timescale  $\langle t_a(x_0) \rangle_1 \approx w_1(x_0)/\mu_1 \equiv \langle t_a(x_0) \rangle_1^{\text{slowest}}$ . The dominance of the single slowest time-scale is fully corroborated by simulations as depicted in Fig. 2b (compare solid black line and dash-dotted magenta line). Notably, the approximation  $\langle t_a(x_0) \rangle_1 \approx w_1(x_0)/\mu_1 (\ll w_2(x_0)/\mu_2)$  can be accurate even if the barriers are not located between  $x_0$  and  $a$  as can be seen in Fig. 2 for  $x_0 \gtrsim 1$  (see Fig. 1a for potential landscape). This can be explained intuitively by the fact that  $w_1(x_0)$  is approximately the splitting probability that the particle will reach the deepest potential well at  $x^\dagger \approx -1.8$  before hitting the target  $a = a_3$ , multiplied by the average time to leave the deepest basin in the potential, which is  $1/\mu_1$  [26].

In the  $N$  particle setting the “slowest” first passage rate is simply  $\mu_1^{(N)} = N\mu_1$ , such that the long-time limit of the first passage time density is given by  $\wp_a^{(N)}(t|x_0) \simeq w_1^{(N)}(x_0) \mu_1^{(N)} e^{-\mu_1^{(N)} t}$  with weight  $w_1^{(N)}(x_0) = w_1(x_0)^N$ . Utilizing only long-time asymptotics in the  $N$ -particle system gives

$$\langle t_a(x_0) \rangle_N^{\text{slowest}} = \frac{w_1(x_0)^N}{N\mu_1}. \quad (15)$$

Comparing the exact  $\langle t(x_0) \rangle_N$  with this approximation in terms of  $\phi_N = \langle t(x_0) \rangle_N / \langle t(x_0) \rangle_N^{\text{slowest}}$  (see Fig. 2c) reveals, however, that the long-time approximation can be orders of magnitude off, despite its accuracy in the single particle setting. In particular, it underestimates  $\langle t(x_0) \rangle_N$  for distant  $x_0$  up to approximately the point  $x_0 \approx -1.1$  (see curves with  $1 \leq N \leq 20$ ), where  $w_2$  changes sign, where from it overestimates  $\langle t(x_0) \rangle_N$ . Increasing  $N$  further beyond  $N > 20$  shift the first passage towards shorter time scales, rendering higher modes corresponding to  $w_{k \geq 3}$  more relevant, which finally yields a systematically longer mean first passage time than expected from the single times-scale estimate (see magenta line with filled rectangles,



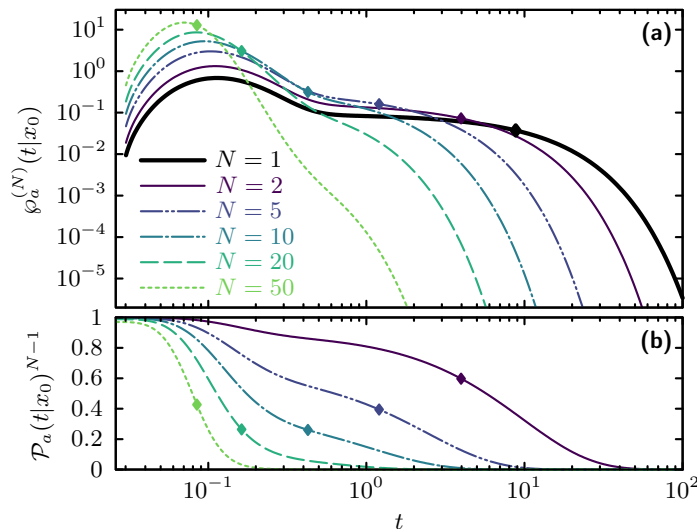


**Figure 3.** Narrowing of the first passage time density in the few-encounter limit. (a)  $N$ -particle density for  $x_0 \rightarrow a_1$ . The thick solid line corresponds to the solid blue line in Fig. 1d. The diamonds depict the respective mean first passage times  $\langle t_a(x_0) \rangle_N$ . (b) The survival probability  $P_a(t|x_0)^{N-1}$  that none of the remaining  $N - 1$  particles has reached the target. According to Eq. (12) each colored curve in (a) is the product of the thick curve  $N = 1$  and the corresponding survival probability in (b).

$N = 100$ , in Fig. 2c). The large discrepancy as a result of neglecting direct and locally indirect trajectories grows further with increasing  $N$ , and highlights the importance of understanding the full first passage time statistics. The lines in Fig. 2c are obtained with the duality relation presented in Sec. 2 and are fully corroborated by Brownian dynamics simulations (symbols).

We now inspect the shape of the distribution upon increasing the number of particles in Fig. 3. We can identify in Fig. 3a two competing effects that eventually lead to a canonical narrowing of the first passage time distribution for  $N \gg 1$ . First, according to Eq. (13) the  $N$ -particle density is proportional to  $\mathcal{P}_a(t|x_0)^{N-1}$ , with  $\mathcal{P}_a(t|x_0)$  being a strictly monotonic decaying function that formally satisfies  $\mathcal{P}_a(0|x_0) = 1$  and  $\mathcal{P}_a(\infty|x_0) = 0$ . By increasing the number of particles  $N$  the weight of the survival probability  $\mathcal{P}_a(t|x_0)^{N-1}$  is progressively shifted towards shorter time-scales (see Fig. 3b), i.e., the long-time asymptotics are shifted towards shorter times for increasing  $N$ , thereby decreasing the width of the probability density. Second, at short times the single-particle first passage probability density for generic diffusion process vanishes [13, 65, 66],  $\lim_{t \rightarrow 0} \varphi_a(t|x_0) = 0$ . We will refer to this feature as the “short-time cutoff”, which according to Eq. (13) prevails for any number of particles  $N$ . Hence the combination of the suppression of long-time asymptotics and the short-time cutoff eventually inevitably leads to a narrowing of the first passage time distribution, irrespective of the details of the underlying dynamics. Further studies specifically targeting the short time limit of first passage time distributions can be found in [65, 66].

In general, the ‘ $N$ -particle’ first passage problem is essential for describing

nucleation kinetics, since the occurrence of the first stable nucleus triggers the spontaneous growth of the new phase (see e.g. [65, 66]). A particular form thereof is the occurrence of misfolding-triggered protein aggregation resulting in many diseases [61–64]. Namely, in many-protein systems the free energy minimum does not correspond to a folded state, but rather to an aggregate of misfolded proteins [63, 64]. Misfolding of a single protein, which indeed occurs by slow diffusion in a rough energy landscape [61, 62], seeds aggregation similar to a nucleation phenomenon. To predict the onset of aggregation and hence disease from the protein’s energy landscape, an understanding of the full first passage time statistics is required, and our work provides the foundations to do so. In the following section we briefly show that our exact theory from Sec. 2 can also be applied to systems with truly rugged energy landscapes.

#### 4. Rugged energy landscapes

In the previous section we have demonstrated that our theory from Sec. 2 can readily be used to obtain first passage time densities for multi-well barrier crossing problems with barrier heights  $> k_B T$ . Moreover, we have discussed the few-encounter limit, for which it is imperative to have access to the full first passage time distribution, since any attempt to explain many-particle first passage kinetics by single-particle moments are prone to fail.

To model a rugged energy landscape containing, in addition to high barriers, also barriers which are  $\lesssim k_B T$ , we use a parabolic potential plus a Karhunen-Loève expansion of a realization of a Brownian motion

$$U(x) = x^2/4 + \sum_{k=1}^K z_k \frac{\sin[(2k-1)x]}{(2k-1)}, \quad (16)$$

where we have truncated the potential after  $K$  terms and where  $z_k$  are Gaussian random numbers. Once  $z_k$  are generated we keep them constant. In Fig. 4a we depict the potential generated from Eq. (16) with  $K = 16$ . As before, we determine the eigenvalues  $\{\lambda_k\}$  and eigenfunctions  $\{\psi_k^R(x)\}$  of the relaxation process with  $\psi_0^R$  being the equilibrium Boltzmann density (see left panel of Fig. 4). Exploiting the theory from Sec. 2 we obtain the first passage time density  $\wp_a(t|x_0)$  in Fig. 4c (see solid black line), which is corroborated by extensive Brownian dynamics simulations (see blue open circles). The inset of Fig. 4c depicts the first passage density on a linear scale. In order to indicate the short-time cutoff, which is dominated by diffusive transport, we also plot the short time asymptotic for free diffusion ( $U(x) = 0$ ). In Fig. 4d we depict the corresponding  $N$ -particle first passage time densities for the few-encounter limit, which clearly reveal the drastic narrowing of the first passage time distribution arising from the aforementioned interplay between the diffusive short-time cutoff and the suppression of the long-time asymptotics for increasing  $N$ . This example illustrates that our theory can readily be applied to arbitrarily rough potential landscapes.

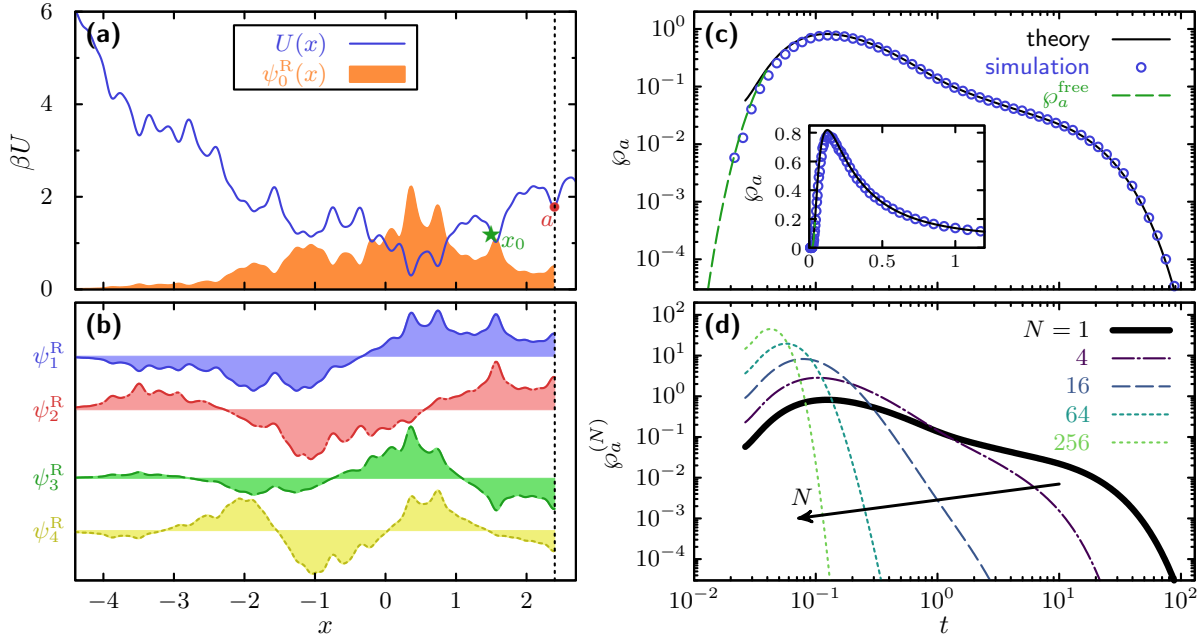


**Figure 4.** First passage in a rugged energy landscape. (a) Potential from Eq. (16) with the corresponding equilibrium measure  $\psi_0^R(x) \propto P_{\text{eq}}(x)$ ,  $K = 16$  and  $(z_1, \dots, z_{16}) = (-0.2, -0.83, -0.93, 1.05, -0.79, 0.55, 0.61, 1.96, -0.88, -1.41, -1.53, -0.31, -0.75, -0.43, -0.46, 1.34)$ . The first passage from  $x_0 = 1.5$  to  $a = 2.4$  is considered. (b) First four excited-state eigenfunctions of the relaxation process. (c) First passage time density  $\varphi_a(t|x_0)$  on a log-log-scale with the corresponding plot on a linear scale depicted in the inset. The solid black line is determined using the duality Eqs. (5-9) while the blue symbols are obtained by simulating  $10^6$  trajectories. The dashed green line corresponds to the short-time asymptotics of the density  $\varphi_a^{\text{free}}(t|x_0) = (2\sqrt{\pi t^3})^{-1}|a - x_0| \exp[-(a - x_0)^2/(4t)]$  for a free Brownian motion ( $U(x) = 0$ ; see, e.g., Ref. [26]). (d)  $N$ -particle first passage time density  $\varphi_a^{(N)}(t|x_0)$ .

## 5. Large deviation limit

For single-particle problems the mean first passage time as well as higher moments are typically dominated by the long-time asymptotics of the first passage time distribution, which we have also demonstrated in Fig. 2b for the triple-well potential. The long-time limit is encoded in the principal first passage eigenvalue  $\mu_1$ . As we demonstrate in Appendix A, the principal eigenvalue  $\mu_1$  can be obtained in a simplified manner by formally setting  $\bar{\mu}_k = 0$  and  $k^* = 0$  in Eq. (7). Moreover, a powerful approximation can be obtained by truncating in Eq. (7) all coefficients with  $n > 2$  (for a formal justification see last paragraph of Appendix A),

$$\mu_1 \simeq \tilde{\mu}_1 = \frac{\sigma_1(a)}{2\sigma_2(a)} \left[ \sqrt{1 + 4 \frac{P_{\text{eq}}(a)\sigma_2(a)}{\sigma_1(a)^2}} - 1 \right], \quad (17)$$

where we introduced  $\sigma_n(a) \equiv \sum_{l \geq 1} \langle a | \psi_l^R \rangle \langle \psi_l^L | a \rangle / \lambda_l^n$ . Since Eq. (17) is derived from a Taylor expansion around  $s = 0$  (see Eq. (A.7)) it is expected to be quite accurate as soon as the formal condition  $\mu_1 \ll \lambda_1$  is met, which in turn translates self-consistently

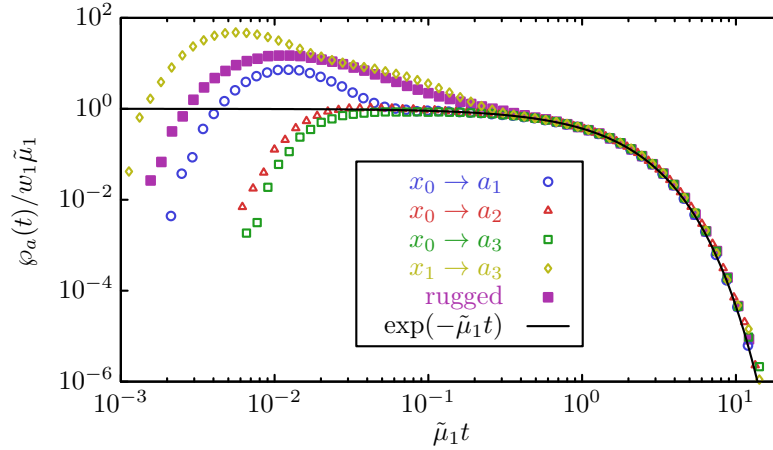


**Figure 5.** Rescaled first passage time probability density,  $\varphi(t)/(w(x_0)\tilde{\mu}_1)$ , obtained by rescaling the simulation results from Fig. 1d (colored open symbols) and Fig. 4c (filled magenta rectangles) by Eqs. (9) and (17). The line denotes a unit exponential.

into  $\tilde{\mu}_1 \ll \lambda_1$ . The relative error  $\epsilon = |\mu_1 - \tilde{\mu}_1|/\mu_1$  is expected to scale as  $\epsilon \propto (\tilde{\mu}_1/\lambda_1)^2$ . For example, in the presence of at least one high barrier and as long as  $a$  is not the deepest point of  $U(x)$  the condition  $\lambda_1 \gg \mu_1$  is indeed satisfied (see, e.g. Fig. 1a,c). Thus, rescaling  $\varphi_a(t)$  according to Eq. (17), all curves must collapse for long times onto a unit exponential  $\varphi_a(t = \theta/\tilde{\mu}_1)/(w(x_0)\tilde{\mu}_1) = e^{-\theta}$ , which is indeed fully confirmed in Fig. 5. The relative errors for the triple-well potential (see open colored symbols) are strictly bounded,  $|\mu_1 - \tilde{\mu}_1|/\mu_1 < 0.02$  for any  $a$ .

More generally, Eq. (17) holds for relaxation spectra obtained under a reflecting boundary at  $a$ , as well as for natural boundary conditions if there is no deeper minimum beyond  $a$ . If furthermore  $P_{\text{eq}}(a) \rightarrow 0$  in Eq. (17) (i.e. the case of 'rare-event' absorption), then  $\tilde{\mu}_1 \simeq P_{\text{eq}}(a)/\sigma_1(a)$ , where particularly

$$\sigma_1(a) = \int_0^\infty [P(a, t|a) - P_{\text{eq}}(a)] dt. \quad (18)$$

Eq. (17) generalizes the 'Poissonization' phenomenon observed in [26, 27]. We note that Eq. (17) can also accurately describe the long-time first passage asymptotics in rugged energy landscapes with an arbitrary number of lower barriers (i.e.  $< k_B T$ ; see closed magenta rectangles in Fig. 5). Further technical remarks including an extension to discrete state systems can be found in [59].

## 6. Conclusion

This paper establishes rigorously the duality between relaxation and first-passage processes for ergodic reversible Markovian dynamics. Based on the duality, an intuitive explanation of first passage time statistics in general rugged energy landscapes is provided. The full first passage time statistics are shown to be required for explaining correctly the kinetics in the few-encounter limit – particularly relevant cases thereof

are the triggering of diseases by protein misfolding and related nucleation-limited phenomena. In addition, we obtained accurate large deviation asymptotics dominating the mean first passage time, which emerge from a time-scale separation in the relaxation process. We show in [59] that all concepts presented here can readily be extended to discrete state-space network dynamics, which, *inter alia* extends the duality between first passage and relaxation to higher dimensional networks. Notably, they allowed us to determine, for the first time, analytically the full first passage time statistics of the Ornstein-Uhlenbeck process (see [59]). Our work provides an exact unified framework for studying the full statistics of first passage time under detailed balance conditions. Generalizations to irreversible dynamics will be pursued in our future studies.

## Acknowledgments

The financial support from the German Research Foundation (DFG) through the *Emmy Noether Program "GO 2762/1-1"* (to AG) is gratefully acknowledged.

## Appendix A. Proof of the duality

In this appendix we sketch the proof of the duality, which allows us to determine analytically the first passage time distribution from the corresponding relaxation spectrum, i.e., the weights  $\{w_k\}$  (not necessarily positive) and first passage rates  $\{\mu_k\}$  that satisfy

$$\tilde{\varphi}_a(s|x_0) = \sum_{k>0} w_k(x_0) \frac{\mu_k}{\mu_k + s} \quad (\text{A.1})$$

directly from the relaxation spectrum  $\{\lambda_k, \psi_k^R\}$ . A detailed technical derivation including an extension to discrete state dynamics can also be found in [59]. Since the first passage eigenvalues  $\mu_k$  correspond to the poles of  $\tilde{\varphi}_a(s|x_0)$  and the renewal theorem states  $\tilde{\varphi}_a(s|x_0) = \tilde{P}(a, s|x_0)/\tilde{P}(a, s|a)$ , our goal will be to find the zeros of

$$\tilde{P}(a, s|a) = \sum_{l \geq 0} \frac{\langle a|\psi_l^R\rangle\langle\psi_l^L|a\rangle}{s + \lambda_l}, \quad (\text{A.2})$$

where the reversibility of the Fokker-Planck operator imposes  $\langle a|\psi_l^R\rangle\langle\psi_l^L|a\rangle > 0$  for all relevant relaxation modes  $\langle a|\psi_l^R\rangle \neq 0$ .

For the  $k$ th first passage rate  $\mu_k$  we introduce the auxiliary functions

$$F(k', s) \equiv (s + \lambda_{k'})\tilde{P}(a, s|a), \quad (\text{A.3})$$

which for any  $k' = k, k-1$  by design are strictly concave  $\partial_s^2 F_{k'} < 0$  within the interval  $-\lambda_k < s < -\lambda_{k-1}$ . We choose  $k^* = k$  or  $k^* = k-1$  such that  $F(k^*(k), s)$  is restricted to be negative at  $s = -\bar{\mu}_k = -(\lambda_k + \lambda_{k-1})/2$ , i.e.,

$$k^*(k) = \begin{cases} k & \text{if } F_k(-\bar{\mu}_k) < 0, \\ k-1 & \text{otherwise.} \end{cases} \quad (\text{A.4})$$

Consequently,  $F(k^*(k), s)$  is both negative and concave between  $s = -\bar{\mu}_k$  and  $s = -\mu_k$ , with  $F(k^*(k), -\mu_k) = 0$ , which implies that any Newton iteration starting from  $\bar{\mu}_k$  will strictly converge towards  $\mu_k$ .

The final step is to use an infinite Newton series – an analytical version of Newton’s iteration – in form of a series of almost triangular matrices [26]. First, we take the Taylor expansion of

$$F(k^*(k), s) = \sum_{n=0}^{\infty} \frac{f_n(k)}{n!} (s + \bar{\mu}_k)^n, \quad (\text{A.5})$$

where  $f_n(k) = \partial_s^n F(k^*(k), s)|_{s=-\bar{\mu}_k}$ , which are explicitly given in Eq. (7). Note that Eq. (A.4) implies  $f_0(k) < 0$ . According to the interlacing theorem in Eq. (4) the Taylor series in Eq. (A.5) converges on the full interval  $-\lambda_k < s < -\lambda_{k-1}$  including the  $s = -\mu_k$ . Furthermore, the auxiliary function from Eq. (A.3) and Eq. (A.4) guarantee the Newton series to converge to the true root  $s = -\mu_k$  at which  $F(k^*(k), -\mu_k) = 0$ . Hence, the  $k$ th first passage rate  $\mu_k$  is exactly and explicitly given by the converging sum Eq. (5).

Having determined the first passage eigenvalue  $\mu_k$  the corresponding weight can simply be determined from  $\tilde{\varphi}_a(s|x_0) = \tilde{P}(a, s|x_0)/\tilde{P}(a, s|a)$  and Eq. (A.1) by using the residue theorem that finally yields

$$w_k(x_0) = \frac{\tilde{P}(a, -\mu_k|x_0)}{\mu_k \partial_s \tilde{P}(a, s|a)|_{s=-\mu_k}}. \quad (\text{A.6})$$

Eq. (A.6) is equivalent to Eq. (9) and completes the proof since all first passage weights  $w_k(x_0)$  and eigenvalues  $\mu_k$  fully characterize the first passage time density  $\wp_a(t|x_0) = \sum_{k>0} w_k(x_0) \mu_k e^{-\mu_k t}$ .

We finally provide some remarks on the principal eigenvalue  $\mu_1$ . If only the principal eigenvalue is of interest the aforementioned discussion can be simplified in the following way. First, we realize that there exist no relaxation eigenvalue, which is smaller than  $\lambda_0$ . Therefore, the simple choice  $k^* = 0$  allows for a Taylor expansion of  $F(k^*=0, s)$  around  $\bar{\mu}_1 = 0$  in Eq. (A.5) that converges on the full interval  $-\lambda_1 \leq s \leq +\lambda_1$ , which includes the lowest first passage eigenvalue  $s = -\mu_1$ . Inserting  $k^* = 0$  and  $\bar{\mu}_1 = 0$  in Eq. (A.5) and using Eq. (7) finally yields

$$F(0, s) = P_{\text{eq}}(a) + \sum_{n=1}^{\infty} (-1)^{n+1} \sigma_n(a) s^n, \quad (\text{A.7})$$

where  $\sigma_n(a) \equiv \sum_{l \geq 1} \langle a | \psi_l^R \rangle \langle \psi_l^L | a \rangle / \lambda_l^n$ , with  $\mu_1$  being the negative zero of  $F(0, s)$ , i.e.  $F(0, -\mu_1) = 0$ . If we truncate the series (A.7) after  $n = 2$  we obtain a simple parabolic equation with the solution  $\tilde{\mu}_1$  given in Eq. (17). Note that Eq. (17) equivalently follows from Eq. (5) if one formally sets therein  $f_n(1) = 0$  for all  $n > 2$  (see also [59]).

## References

- [1] S. Dattagupta, *Relaxation phenomena in condensed matter physics*. Academic Press, Orlando, Florida, 1987.



- [2] M. Doi and S. F. Edwards, *The Theory of Polymer Dynamics*. Oxford University Press, New York, 1986.
- [3] S. F. Edwards, *The Role of Entropy in the Specification of a Powder*, ch. 4, pp. 121–140. Springer, New York, NY, 1994.
- [4] F. Noé, S. Dose, I. Daidone, M. Löllmann, M. Sauer, J. D. Chodera, and J. C. Smith, “Dynamical fingerprints for probing individual relaxation processes in biomolecular dynamics with simulations and kinetic experiments,” *Proc. Natl. Acad. Sci. USA* **108** (2011) 4822–4827.
- [5] H. Chen, E. Rhoades, J. S. Butler, S. N. Loh, and W. W. Webb, “Dynamics of equilibrium structural fluctuations of apomyoglobin measured by fluorescence correlation spectroscopy,” *Proc. Natl. Acad. Sci. USA* **104** (2007) 10459–10464.
- [6] A. M. Walczak, A. Mugler, and C. H. Wiggins, *Analytic Methods for Modeling Stochastic Regulatory Networks*, ch. 13, pp. 273–322. Humana Press, Totowa, NJ, 2012.
- [7] J. Langer, “Statistical theory of the decay of metastable states,” *Ann. Phys.* **54** (1969) 258–275.
- [8] A. Bovier and F. den Hollander, *Metastability: A Potential-Theoretic Approach*. Springer, Cham, 2015.
- [9] G. Biroli and J. Kurchan, “Metastable states in glassy systems,” *Phys. Rev. E* **64** (2001) 016101.
- [10] S. Tănase-Nicola and J. Kurchan, “Topological methods for searching barriers and reaction paths,” *Phys. Rev. Lett.* **91** (2003) 188302.
- [11] S. Tănase-Nicola and J. Kurchan, “Metastable states, transitions, basins and borders at finite temperatures,” *J. Stat. Phys.* **116** (2004) 1201–1245.
- [12] P. Hänggi, P. Talkner, and M. Borkovec, “Reaction-rate theory: fifty years after kramers,” *Rev. Mod. Phys.* **62** (1990) 251–341.
- [13] S. Redner, *A guide to first-passage processes*. Cambridge University press, Cambridge, 2001.
- [14] R. Metzler, G. Oshanin, and S. Redner, eds., *First-Passage Phenomena and Their Applications*. World Scientific Publishing, Singapore, 2014.
- [15] R. Kopelman, “Fractal reaction kinetics,” *Science* **241** (1988) 1620–1626.
- [16] A. Szabo, K. Schulten, and Z. Schulten, “First passage time approach to diffusion controlled reactions,” *J. Chem. Phys.* **72** (1980) 4350–4357.
- [17] O. Bénichou, C. Chevalier, J. Klafter, B. Meyer, and R. Voituriez, “Geometry-controlled kinetics,” *Nat. Chem.* **2** (2010) 472–477.
- [18] E. Ben-Naim, S. Redner, and F. Leyvraz, “Decay kinetics of ballistic annihilation,” *Phys. Rev. Lett.* **70** (1993) 1890–1893.
- [19] G. Oshanin, A. Stemmer, S. Luding, and A. Blumen, “Smoluchowski approach for three-body reactions in one dimension,” *Phys. Rev. E* **52** (1995) 5800–5805.
- [20] O. Bénichou and R. Voituriez, “From first-passage times of random walks in confinement to geometry-controlled kinetics,” *Phys. Rep.* **539** (2014) 225–284.
- [21] T. Guérin, N. Leverrier, O. Bénichou, and R. Voituriez, “Mean first-passage times of non-Markovian random walkers in confinement,” *Nature* **534** (2016) 356–359.
- [22] C. Mejía-Monasterio, G. Oshanin, and G. Schehr, “First passages for a search by a swarm of independent random searchers,” *J. Stat. Mech.* (2011) P06022.
- [23] D. Holcman and Z. Schuss, “Time scale of diffusion in molecular and cellular biology,” *J. Phys. A: Math. Theor.* **47** (2014) 173001.
- [24] A. Godec and R. Metzler, “First passage time distribution in heterogeneity controlled kinetics: going beyond the mean first passage time,” *Sci. Rep.* **6** (2016) 20349.
- [25] A. Godec and R. Metzler, “Optimization and universality of brownian search in a basic model of quenched heterogeneous media,” *Phys. Rev. E* **91** (2015) 052134.
- [26] A. Godec and R. Metzler, “Universal proximity effect in target search kinetics in the few-encounter limit,” *Phys. Rev. X* **6** (2016) 041037.
- [27] A. Godec and R. Metzler, “First passage time statistics for two-channel diffusion,” *J. Phys. A: Math. Theor.* **50** (2017) 084001.
- [28] D. S. Grebenkov, “Universal formula for the mean first passage time in planar domains,” *Phys.*

- Rev. Lett.* **117** (2016) 260201.
- [29] D. S. Grebenkov and G. Oshanin, “Diffusive escape through a narrow opening: new insights into a classic problem,” *Phys. Chem. Chem. Phys.* **19** (2017) 2723–2739.
  - [30] D. S. Grebenkov, R. Metzler, and G. Oshanin, “Towards a full quantitative description of single-molecule reaction kinetics in biological cells,” *Phys. Chem. Chem. Phys.* **20** (2018) 16393–16401.
  - [31] G. Vaccario, C. Antoine, and J. Talbot, “First-passage times in  $d$ -dimensional heterogeneous media,” *Phys. Rev. Lett.* **115** (2015) 240601.
  - [32] D. ben Avraham and S. Havlin, *Diffusion and Reactions in Fractals and Disordered Systems*. Cambridge University Press, Cambridge, 2000.
  - [33] H. C. Berg, *Random walks in biology*. Princeton University Press, 1993.
  - [34] W. J. Bell, *Searching Behaviour*. Springer, Dordrecht, 1990.
  - [35] V. V. Palyulin, A. V. Chechkin, and R. Metzler, “Lévy flights do not always optimize random blind search for sparse targets,” *Proc. Natl. Acad. Sci. USA* **111** (2014) 2931–2936.
  - [36] A. L. Lloyd and R. M. May, “How viruses spread among computers and people,” *Science* **292** (2001) 1316–1317.
  - [37] L. Hufnagel, D. Brockmann, and T. Geisel, “Forecast and control of epidemics in a globalized world,” *Proc. Natl. Acad. Sci. USA* **101** (2004) 15124–15129.
  - [38] R. N. Mantegna and H. E. Stanley, *Introduction to Econophysics*. Cambridge University Press, Cambridge, UK, 2000.
  - [39] A. J. Bray, S. N. Majumdar, and G. Schehr, “Persistence and first-passage properties in nonequilibrium systems,” *Adv. Phys.* **62** (2013) 225–361.
  - [40] S. N. Majumdar and A. J. Bray, “Spatial persistence of fluctuating interfaces,” *Phys. Rev. Lett.* **86** (2001) 3700–3703.
  - [41] S. N. Majumdar and A. Comtet, “Exact asymptotic results for persistence in the Sinai model with arbitrary drift,” *Phys. Rev. E* **66** (2002) 061105.
  - [42] I. Neri, E. Roldán, and F. Jülicher, “Statistics of infima and stopping times of entropy production and applications to active molecular processes,” *Phys. Rev. X* **7** (2017) 011019.
  - [43] J. P. Garrahan, “Simple bounds on fluctuations and uncertainty relations for first-passage times of counting observables,” *Phys. Rev. E* **95** (2017) 032134.
  - [44] E. Roldán and S. Gupta, “Path-integral formalism for stochastic resetting: Exactly solved examples and shortcuts to confinement,” *Phys. Rev. E* **96** (2017) 022130.
  - [45] T. R. Gingrich and J. M. Horowitz, “Fundamental bounds on first passage time fluctuations for currents,” *Phys. Rev. Lett.* **119** (2017) 170601.
  - [46] J. Fuchs, S. Goldt, and U. Seifert, “Stochastic thermodynamics of resetting,” *EPL* **113** (2016) 60009.
  - [47] B. Nguyen, D. Hartich, U. Seifert, and P. De Los Rios, “Thermodynamic bounds on the ultra- and infra-affinity of Hsp70 for its substrates,” *Biophys. J.* **113** (2017) 362–370.
  - [48] D. Wales, *Energy Landscapes: Applications to Clusters, Biomolecules and Glasses*. Cambridge Molecular Science. Cambridge University Press, 2004.
  - [49] H. Kramers, “Brownian motion in a field of force and the diffusion model of chemical reactions,” *Physica* **7** (1940) 284–304.
  - [50] K. Schulten, Z. Schulten, and A. Szabo, “Dynamics of reactions involving diffusive barrier crossing,” *J. Chem. Phys.* **74** (1981) 4426–4432.
  - [51] H. Frauenfelder, S. G. Sligar, and P. G. Wolynes, “The energy landscapes and motions of proteins,” *Science* **254** (1991) 1598–1603.
  - [52] J. N. Onuchic, Z. Luthey-Schulten, and P. G. Wolynes, “Theory of protein folding: The energy landscape perspective,” *Annu. Rev. Phys. Chem.* **48** (1997) 545–600.
  - [53] K. Neupane, A. P. Manuel, and M. T. Woodside, “Protein folding trajectories can be described quantitatively by one-dimensional diffusion over measured energy landscapes,” *Nat. Phys.* **12** (2016) 700.
  - [54] J. P. Garrahan and D. Chandler, “Geometrical explanation and scaling of dynamical

- heterogeneities in glass forming systems,” *Phys. Rev. Lett.* **89** (2002) 035704.
- [55] E. Barkai, E. Aghion, and D. A. Kessler, “From the area under the Bessel excursion to anomalous diffusion of cold atoms,” *Phys. Rev. X* **4** (2014) 021036.
  - [56] B. J. Matkowsky and Z. Schuss, “Eigenvalues of the Fokker–Planck operator and the approach to equilibrium for diffusions in potential fields,” *SIAM J. Appl. Math.* **40** (1981) 242–254.
  - [57] A. J. F. Siegert, “On the first passage time probability problem,” *Phys. Rev.* **81** (1951) 617–623.
  - [58] J. Keilson, “A review of transient behavior in regular diffusion and birth-death processes,” *J. Appl. Prob.* **1** (1964) 247–266.
  - [59] D. Hartich and A. Godec, “Interlacing relaxation and first-passage phenomena in reversible discrete and continuous space Markovian dynamics,” *ArXiv e-prints* (2018) , [arXiv:1802.10049 \[cond-mat.stat-mech\]](#).
  - [60] J. D. Bryngelson and P. G. Wolynes, “Intermediates and barrier crossing in a random energy model (with applications to protein folding),” *J. Phys. Chem.* **93** (1989) 6902–6915.
  - [61] H. Yu, D. R. Dee, X. Liu, A. M. Brigley, I. Sosova, and M. T. Woodside, “Protein misfolding occurs by slow diffusion across multiple barriers in a rough energy landscape,” *Proc. Natl. Acad. Sci. USA* **112** (2015) 8308–8313.
  - [62] D. R. Dee and M. T. Woodside, “Comparing the energy landscapes for native folding and aggregation of PrP,” *Prion* **10** (2016) 207–220.
  - [63] C. M. Dobson, “Protein folding and misfolding,” *Nature* **426** (2003) 884–890.
  - [64] W. Zheng, N. P. Schafer, and P. G. Wolynes, “Free energy landscapes for initiation and branching of protein aggregation,” *Proc. Natl. Acad. Sci. USA* **110** (2013) 20515–20520.
  - [65] N. G. van Kampen, “Short first-passage times,” *J. Stat. Phys.* **70** (1993) 15–23.
  - [66] H. van Beijeren, “The uphill turtle race; on short time nucleation probabilities,” *J. Stat. Phys.* **110** (2003) 1397–1410.